Meshless Simulation of Multi-site Radio Frequency Catheter Ablation through the Fragile Points Method

Konstantinos A. Mountris, Richard Schilling, Alicia Casals, Helge A. Wurdemann

***Abstract*— Computational models for radio frequency catheter ablation (RFCA) of cardiac arrhythmia have been developed and tested in conditions where a single ablation site is considered. However, in reality arrhythmic events are generated at multiple sites which are ablated during treatment. Under such conditions, heat accumulation from several ablations is expected and models should take this effect into account. Moreover, such models are solved using the Finite Element Method which requires a good quality mesh to ensure numerical accuracy. Therefore, clinical application is limited since heat accumulation effects are neglected and numerical accuracy depends on mesh quality. In this work, we propose a novel meshless computational model where tissue heat accumulation from previously ablated sites is taken into account. In this way, we aim to overcome the mesh quality restriction of the Finite Element Method and enable realistic multi-site ablation simulation. We consider a two ablation sites protocol where tissue temperature at the end of the first ablation is used as initial condition for the second ablation. The effect of the time interval between the ablation of the two sites is evaluated. The proposed method demonstrates that previous models that do not account for heat accumulation between ablations may underestimate the tissue heat distribution.**

***Clinical relevance*— The proposed computational model may be used to build and update a heat map for ablation guidance taking into account the contribution from previously ablated sites. Being a meshless model, it does not require significant input from the user during preprocessing. Therefore, it is suitable for application in a clinical setting.**

I. INTRODUCTION

Nowadays radio frequency catheter ablation (RFCA) is widely used for the treatment of patients with arrhythmia that do not respond adequately to anti-arrhythmic drugs. During RFCA, a catheter delivers heat at the arrhythmic regions with the objective to cause permanent lesions and hence halt the arrhythmic events. In order for ablation lesions to be permanent, it is required that tissue temperature rises over 50°C but does not exceed 100°C. Underheating may lead to arrhythmia recurrence, while overheating may lead to health complications such as cardiac perforation [1].

This work has received funding from the European Union's Horizon 2020 research and innovation programme under the Marie Skłodowska-Curie grant agreement PhyNeTouch No 101024463.

Konstantinos A. Mountris is with the department of Mechanical Engineering, University College London, London, United Kingdom. (Email: k.mountris@ucl.ac.uk).

Richard Schilling is with Barts Heart Centre, St Bartholomew's Hospital, London, United Kingdom. (Email: richard.schilling@nhs.net).

Alicia Casals is with Research Center for Biomedical Engineering, Universitat Politecnica de Catalunya, Barcelona, Spain. (Email: alicia.casals@upc.edu).

Helge A. Wurdemann is with with the department of Mechanical Engineering, University College London, London, United Kingdom. (Email: h.wurdemann@ucl.ac.uk).

Monitoring tissue heat distribution during RFCA is of paramount importance. Direct in-vivo tissue heat measurement remains challenging and clinicians rely on catheter-tissue contact force measurements to evaluate indirectly the tissue heat distribution. However, force-heat relationship is not linear and the deposited heat cannot be predicted accurately. On the other hand, computational modelling demonstrates high predicting capacity of tissue heating under different ablation conditions [2]. Available computational models employ the Finite Element Method (FEM) to solve the Pennes bioheat equation for RFCA simulation. Tissue deformation during catheter contact and cooling effects due to blood flow are also taken into account. However, FEM models require a high-quality mesh to ensure good accuracy during simulation. Moreover, they have been tested only in single-site ablation protocols. While such protocols are useful for experimental validation, they don't account for heat accumulation during the ablation of multiple sites which is common in clinical practice.

In this work, we developed a meshless model taking into account tissue heat accumulation during multi-site ablation under the hypothesis that accumulated heat from previously ablated sites affects the heat distribution and lesion formation. We employ the meshless Fragile Points Method (FPM) [3] to solve the Pennes bioheat equation taking into account the non-linear deformation of the tissue during contact with the catheter [4]. FPM is a novel meshless method that has been proven to provide results with similar accuracy to FEM while alleviating the requirement of a good quality mesh [5]. Therefore, it is more suitable for clinical application.

II. CATHETER ABLATION MESHLESS MODEL

Being a meshless method, the Fragile Points Method (FPM) does not require a mesh discretization. The domain of interest Ω is discretized by a set of randomly distributed points. Conforming non-overlapping subdomains that enclose these points are then defined. Simple discontinuous polynomials that are defined in compact support domains are used as approximation. In FPM, the trial function u_h for a general field variable u is defined in terms of u and its gradient ∇u. For a given subdomain E_0 including a point P_0, u_h is obtained by:

$$u_h(\boldsymbol{x}) = u_0 + (\boldsymbol{x} - \boldsymbol{x}_0) \cdot \nabla u\Big|_{P_0}, \tag{1}$$

where $\boldsymbol{x}_0$, $\boldsymbol{x}$ are the coordinates vectors of P_0 and any point in subdomain E_0, respectively and u_0 is the value of u_h at P_0. The gradient $\nabla u\Big|_{P_0}$ is unknown and it is

computed using the Generalized Finite Difference (GFD) method [7]. For details on the computation of $\nabla u\Big|_{P_0}$ see [6]. The polynomials can be used both as trial and test functions to formulate the Galerkin weak form similar to FEM. Heat distribution during ablation is modelled by the Pennes bioheat equation:

$$\begin{aligned} \rho c(T)\frac{\partial T}{\partial t} - \nabla\cdot(k(T)\nabla T) = q \quad & \text{in } \Omega \\ T = T_D \quad & \text{in } \Gamma_D \\ k(T)\nabla T\cdot \boldsymbol{n} = 0 \quad & \text{in } \Gamma_N \end{aligned} \tag{2}$$

where ρ denotes density, $c(T)$ specific heat, and $k(T)$ thermal conductivity. The heat source $q = \sigma(T)|\nabla\Phi|^2$ is generated by the catheter's electrical field, with $\sigma(T)$ being the electrical conductivity and Φ the electrical potential. T_D denotes the prescribed temperature at the Dirichlet boundary Γ_D, $\boldsymbol{n}$ denotes the outward normal at the Neumann boundary Γ_N. To obtain the FPM weak form, we introduce the discontinuous polynomials in Equation (2) and we integrate by parts. Due to the discontinuity of the polynomial functions, the FPM weak form is inconsistent and numerical flux correction is employed to restore its consistency [8]. Employing the Interior Penalty (IP) numerical flux correction [9] with penalty coefficient η, we obtain after rearranging:

$$\begin{aligned} &\sum_{E\in\Omega}\int_E \rho c v\frac{\partial T_h}{\partial t}d\Omega + \int_E k\nabla v\nabla T_h d\Omega - \\ &\sum_{e\in\Gamma_h}\int_e \{k\boldsymbol{n}\nabla T_h\}[\![v]\!]d\Gamma - \sum_{e\in\Gamma_h}\int_e \{k\boldsymbol{n}\nabla v\}[\![T_h]\!]d\Gamma + \\ &\sum_{e\in\Gamma_h}\frac{\eta}{h_e}\int_e [\![T_h]\!][\![v]\!]d\Gamma = 0, \end{aligned} \tag{3}$$

where the jump $[\![\ ]\!]$ and average $\{\ \}$ operators, $\forall w\in\mathbb{R}$ are:

$$[\![w]\!] = \begin{cases} w|_e^{E1} - w|_e^{E2} & e\in\Gamma_h \\ w|_e & e\in\Gamma_N \end{cases}, \tag{4}$$

$$\{w\} = \begin{cases} \frac{1}{2}\left(w|_e^{E1} + w|_e^{E2}\right) & e\in\Gamma_h \\ w|_e & e\in\Gamma_N \end{cases}. \tag{5}$$

e denotes an internal boundary where continuity is restored ($e\in\partial E_1\cap\partial E_2$) and ∂E_1, ∂E_2 denote boundaries of the subdomains E_1, E_2. The same approach is used to obtain the distributed heat source by solving the electric field problem:

$$\begin{aligned} \nabla\cdot(\sigma(T)\nabla\Phi) = 0 \quad & \text{in } \Omega \\ \Phi = \Phi_D \quad & \text{in } \Gamma_D \\ \sigma\nabla\Phi\cdot\boldsymbol{n} = 0 \quad & \text{in } \Gamma_N \end{aligned} \tag{6}$$

Employing the FPM discontinuous polynomials and the IP numerical flux correction, we obtain the consistent Galerkin weak-form of the electrical problem:

$$\begin{aligned} &\sum_{E\in\Omega}\int_E \sigma\nabla v\nabla\Phi_h d\Omega - \sum_{e\in\Gamma_h}\int_e \{\sigma\boldsymbol{n}\nabla\Phi_h\}[\![v]\!]d\Gamma - \\ &\sum_{e\in\Gamma_h}\int_e \{\sigma\boldsymbol{n}\nabla v\}[\![\Phi_h]\!]d\Gamma + \sum_{e\in\Gamma_h}\frac{\eta}{h_e}\int_e [\![\Phi_h]\!][\![v]\!]d\Gamma = 0. \end{aligned} \tag{7}$$

Tissue deformation due to catheter contact is accounted by solving the large deformation boundary problem:

$$\begin{aligned} \nabla_0\cdot\boldsymbol{P} + \rho_0\boldsymbol{b} = \rho_0\ddot{\boldsymbol{u}} \quad & \text{in } \Omega_0 \\ \boldsymbol{u} = \bar{\boldsymbol{u}} \quad & \text{in } \Gamma_D \\ \boldsymbol{P}\cdot\boldsymbol{n}_0 = \bar{\boldsymbol{t}} \quad & \text{in } \Gamma_N \end{aligned} \tag{8}$$

where $\boldsymbol{P}$ is the first Piola-Kirchhoff stress tensor, $\rho_0\boldsymbol{b}$ is the body forces vector, $\ddot{\boldsymbol{u}}$ is the second time derivative of displacement, and $\boldsymbol{n}_0$ is the outward unit surface normal of the initial configuration. Following the implementation described in [4], the consistent FPM formulation of the large deformation problem is given by:

$$\begin{aligned} &\sum_{E\in\Omega_0}\int_E \boldsymbol{S}:\delta\boldsymbol{E}d\Omega - \sum_{E\in\Omega_0}\int_E \rho_0(\boldsymbol{b}-\ddot{\boldsymbol{u}}^h)\cdot\boldsymbol{v}d\Omega - \\ &\sum_{e\in\Gamma_t}\int_e \bar{\boldsymbol{t}}\cdot\boldsymbol{v}d\Gamma - \sum_{e\in\Gamma_h}\int_e \boldsymbol{t}^*\cdot[\![\boldsymbol{v}]\!]d\Gamma = 0, \end{aligned} \tag{9}$$

where $\boldsymbol{S}$ denotes the second Piola-Kirchhoff stress tensor, $\boldsymbol{E}$ denotes the Green-Lagrange strain tensor, and $\boldsymbol{t}^*$ is the numerical flux correction given by the incomplete interior penalty Galerkin (IIPG) method [10]. Catheter-tissue contact is modeled using a master-slave approach where tissue nodes penetrating the surface of the catheter during indentation are projected back to the catheter's surface. For additional details on FPM implementation of large deformation, see [4].

III. Multi-site ablation

1) Modelling approach: Multi-site ablation modelling requires to take into account heat accumulation from multiple ablated sites. The common approach to sum the contribution of individual heat maps could not be applied effectively since it does not take into account temporal changes in the temperature distribution. Ablation times are usually as large as 30 s or more and during this time cooling at the previously ablated sites is expected. If this phenomenon is not taken into consideration, it is expected that heat distribution map will be overestimated. Therefore, we proposed a different approach where tissue temperature from previously ablated sites is introduced in the computational model as initial condition. The simulation of the heat distribution at each ablation starts from a temperature state that depends on the previously ablated sites. Furthermore, we consider time-dependent Dirichlet conditions allowing to take into account the time interval between the start and the end of the ablation of different sites. Given two ablation sites s1, s2 and ablation time $t_a = 30$s per ablation site, we have $T_{s2}(t_s) = T_{s1}(t_e)$, where T_{s1}, T_{s2} denote the temperature at ablation sites s1, s2 respectively. t_s and $t_e = t_s + t_a$ denote the starting and ending time of the ablation at a given site. Since the heat source in our model is given by the catheter's electric field (Equation (2)), we solve the electric problem using the time-dependent Dirichlet conditions given by:

$$\Phi = \Phi_D u(t - t_s) \text{ in } \Gamma_D \tag{10}$$

where $u(t-t_s)$ is the step function:

$$u(t-t_s)=\begin{cases}1 & \text{if } t\geq t_s\\ 0 & \text{if } t<t_s\end{cases} \tag{11}$$

2) Model evaluation protocol: We considered an ablation protocol with two ablation sites of a 3D block of porcine ventricular tissue with dimensions $40\times40\times20$ mm and temperature dependent parameters. Density $\rho = 1076$ kgm^{-3}, initial specific heat $c_0 = 3017$ Jkg^{-1}K, initial thermal conductivity $k_0 = 0.518$ Wm^{-1}K, and initial electrical conductivity $\sigma_0 = 0.54$ Sm^{-1}. The ablation sites were located at the top tissue surface such as s1 $= (0,-1,20)$ mm and s2 $= (0,1,20)$ mm. Ablation time was $t_a = 30$ s for both s1, s2. Ablation simulations were performed using the Abbott ThermoCool© catheter. Temperature $T = 37$°C was imposed as boundary condition at all tissue surfaces. The surface of the catheter was held at $T = 22$°C. The electrical potential at the bottom tissue surface was set $\Phi = 0$ V and $\Phi = 20$ V at the surface of the catheter's electrode. Simulations were performed with catheter indentation at perpendicular position and rotated around the x-axis by a 30° angle at both sites. To distinguish between the different simulations we use the abreviation $R_x = a°$, where x denotes the ablation site and $a°$ the catheter rotation angle at the given site. For instance, $R_{s1} = 0°$, $R_{s2} = 0°$ denotes the simulation where the catheter was perpendicularly indented at both s1, s2 sites. Similarly, $R_{s1} = 30°$, $R_{s2} = -30°$ denotes the simulation where the catheter was indented at an angle of 30° around x-axis at s1 site and $-30°$ around x-axis at the s2 site. The catheter indentation force was $F = 20$g in all simulations.

IV. RESULTS

The ablation lesion at site s2 from single-site ablation (single) simulation was compared with multi-site ablation simulation results. Multi-site ablation was modelled with the proposed approach where temperature distribution from site s1 was used as initial condition (multi-init). Heat maps summation (multi-sum) protocol was also used for completeness. The region of the tissue receiving $T \geq 50$°C was considered as lesion since above 50°C the tissue heat damage was permanent. Characteristics such as width (W), depth (D), and maximum temperature (T_{max}) were computed to compare the heat maps obtained from the single, multi-init, and multi-sum simulations. Three different catheter rotation angles at s1, s2 were considered during simulations. These were namely ($R_{s1} = 0°$, $R_{s2} = 0°$), ($R_{s1} = 30°$, $R_{s2} = 30°$), and ($R_{s1} = 30°$, $R_{s2} = -30°$). Differences in the lesion characteristics between single and multi-init protocols were significant in all simulations. The difference was up to 17.6% for W, 24.4% for D, and 6.1% for T_{max} in the case of vertical catheter indentation ($R_{s1} = 0°$, $R_{s2} = 0°$). Similar results were demonstrated in ($R_{s1} = 30°$, $R_{s2} = 30°$), and ($R_{s1} = 30°$, $R_{s2} = -30°$) simulations and are given in Table I. In Figure 1, $T \geq 50$°C isolines are provided for single- and multi-site ablation protocols for catheter rotation angles $R_{s1} = 0° - R_{s2} = 0°$.

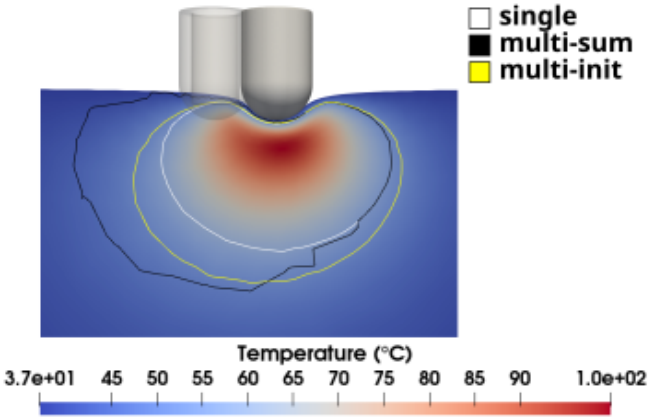

Fig. 1: $T \geq 50$°C isolines for single- and multi-site ablation for perpendicular catheter indentation ($R_1 = 0°$, $R_2 = 0°$). The lesion in single ablation (white) is underestimated compared to multi-init simulation (yellow).

TABLE I: Lesion characteristics for (single); multi-site initial condition (multi-init); summation (multi-sum) protocols.

	single	**multi-sum**	**multi-init**
$R_{s1} = 0°$, $R_{s2} = 0°$			
Width (mm)	7.4	10.5	8.7
Depth (mm)	4.1	5.6	5.1
T_{max} (°C)	90.7	168.3	96.2
$R_{s1} = 30°$, $R_{s2} = 30°$			
Width (mm)	7.2	9.9	8.3
Depth (mm)	4.1	5.4	5.0
T_{max} (°C)	88.0	166.5	93.2
$R_{s1} = 30°$, $R_{s2} = -30°$			
Width (mm)	6.9	10.1	7.9
Depth (mm)	3.8	5.4	4.7
T_{max} (°C)	78.3	158.2	82.8

The effect of the time interval between the end of the first ablation and the beginning of the second was also investigated for the multi-init protocol. A time interval t_i = 0, 2, 4 s was considered to evaluate any differences in the lesion characteristic due to the temporal hysterisis between the two ablations. This effect was investigated considering the same catheter rotation angles as previously. A decrease in the values of the lesion characteristics was observed for the given time intervals. When $t_i = 4$ s was used, there was a decrease down to 3.4% for W. D was decreased down to 2.1% and T_{max} down to 1.0%. A summary of the lession characteristics for the different time intervals is given in Table II. In Figure 2 is given the $T \geq 50$°C isoline for the simulation with catheter rotation angles $R_{s1} = 30°$, $R_{s2} = -30°$ and $t_i = \{0, 2, 4\}$ s.

V. DISCUSSION

In this study, a novel meshless FPM computational model to simulate multi-site ablation was presented. Ablation lesion characteristics were compared between a single-site and two different multi-site protocols. One multi-site protocol considered the simple approach of summing individual heat

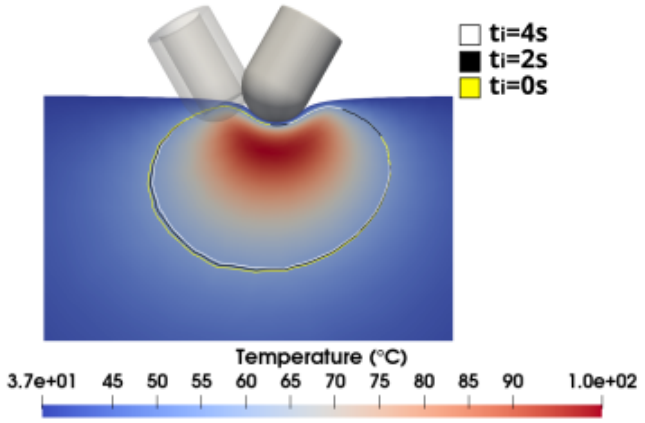

Fig. 2: $T \geq 50$°C isolines for multi-init protocol with time interval $t_i = 0, 2, 4$ s. The lesion is reduced as t_i increases.

TABLE II: Lesion characteristics for multi-init ablation for different time intervals (t_i) and catheter rotation angles.

	$t_i = 0$s	$t_i = 2$s	$t_i = 4$s
$R_{s1} = 0°$, $R_{s2} = 0°$			
Width (mm)	8.7	8.6	8.4
Depth (mm)	5.1	5.0	5.0
$\mathbf{T_{max}}$ (°C)	96.2	96.1	95.9
$R_{s1} = 30°$, $R_{s2} = 30°$			
Width (mm)	8.3	8.2	8.1
Depth (mm)	5.0	4.9	4.9
$\mathbf{T_{max}}$ (°C)	93.2	92.6	92.3
$R_{s1} = 30°$, $R_{s2} = -30°$			
Width (mm)	7.9	7.8	7.7
Depth (mm)	4.7	4.6	4.6
$\mathbf{T_{max}}$ (°C)	82.8	82.6	82.4

maps from single-site ablations. The second protocol used the temperature distribution from previous ablations as an initial condition for the next ablation. The comparison of lesion characteristics between single- and multi-site protocols revealed that the size of the obtained lesion from single-site ablation was underestimated. As shown in Figure 1, the lesion for the multi-init protocol is larger compared to the single protocol since heat from the previous ablation is accumulated. The lesion at the s2 ablation site is extended towards the previously ablated site (site s1).

While max temperature difference between the single and multi-init maps was in the range 5.7% - 6.1%, the width of the lesion was larger in multi-init maps by a range of 14.5% - 17.6%. Similarly, the depth of the lesion was larger in the range of 22.0% - 24.4%. These findings, demonstrate that in multi-site ablation conditions, the width and depth of the lesion are significantly higher compared to single-site ablation. This could mean that taking into account multi-site ablation conditions transmural lesions could be formed for lower tissue temperatures. Therefore, the applied multi-site ablation protocol is important to ensure accurate results. The proposed multi-init approach generated realistic heat maps similar to the single-site approach in terms of shape and temperature distribution pattern. However, the multi-sum approach generated lesions of unrealistic shape that were significantly overestimated.

The comparison of different time intervals between the end of the s1 ablation and the beginning of the s2 ablation, revealed that lesion characteristics are reduced as the time interval increases. However, this decrease was small for time intervals up to 4s. This means that even when there is a time interval between the two ablations the lesion characteristics are significantly different from the ones obtained from a single-site ablation. Therefore, multi-site ablation simulation is required to ensure accurate heat distribution estimation.

VI. CONCLUSION

The FPM was used for the first time to simulate catheter ablation. The proposed model took into account tissue temperature accumulation from ablation at previous sites by setting an appropriate initial condition for the next site's ablation. It was demonstrated that lesion formation was significantly underestimated when multi-site ablation effects were neglected even when there was a time interval between the two ablations. We believe that the proposed algorithm may be proven a useful tool for multi-site ablation simulation that can enable accurate heat distribution prediction and assist decision making during clinical applications.

REFERENCES

[1] F. Akca, P. Janse, D. Theuns, and T. Szili-Torok, A prospective study on safety of catheter ablation procedures: contact force guided ablation could reduce the risk of cardiac perforation, International Journal of Cardiology, vol. 179, 2015.

[2] A. Petras, L. Massimiliano, J.M. Guerra, J. Jansson, and L. Gerardo-Giorda, Luca, A computational model of open-irrigated radiofrequency catheter ablation accounting for mechanical properties of the cardiac tissue, International Journal for Numerical Methods in Biomedical Engineering, vol. 35, 2019.

[3] Y. Guan, and S.N. Atluri, Meshless fragile points methods based on Petrov-Galerkin weak-forms for transient heat conduction problems in complex anisotropic nonhomogeneous media, International Journal for Numerical Methods in Engineering, vol. 122, 2021.

[4] K.A. Mountris, M. Li, R. Schilling, L. Dong, S.N. Atluri, A. Casals, H.A. Wurdemann, An Explicit Total Lagrangian Fragile Points Method for Finite Deformation of Hyperelastic Materials, arXiv preprint, arXiv:2208.05306, 2022.

[5] K.A. Mountris, D. Leiting, Y. Guan, S.N. Atluri, E. Pueyo, A meshless fragile points method for the solution of the monodomain model for cardiac electrophysiology simulation, Journal of Computational Science, vol. 65, 2022.

[6] L. Dong, T. Yang, K. Wang, and S.N. Atluri, A new Fragile Points Method (FPM) in computational mechanics, based on the concepts of Point Stiffnesses and Numerical Flux Corrections, Engineering Analysis with Boundary Elements, vol. 107, 2019.

[7] T. Liszka, and J. Orkisz, The finite difference method at arbitrary irregular grids and its application in applied mechanics, Computers & Structures, vol. 11, 1980.

[8] D.N. Arnold, F. Brezzi, B. Cockburn, L. Marini, and L. Donatella, Unified analysis of discontinuous Galerkin methods for elliptic problems, SIAM journal on numerical analysis, vol. 39, 2002.

[9] I. Mozolevski, E. Süli, and P.R. Bösing, hp-version a priori error analysis of interior penalty discontinuous Galerkin finite element approximations to the biharmonic equation, Journal of Scientific Computing, vol. 30, 2007.

[10] K. Wang, B. Shen, M. Li, L. Dong, and S.N. Atluri, A Fragile Points Method, with an interface debonding model, to simulate damage and fracture of U-notched structures, International Journal for Numerical Methods in Engineering, vol. 123, 2022.